Supplementary Information

Atomic-scale investigation on the electronic states in one-dimensional π-d conjugated metal-organic framework

Nuoyu Su,[a,b#] Tingfeng Zhang,[c#] Weiliang Zhong,[a] Guangyao Miao,[a] Jiandong Guo,[a,b] Zhengfei Wang,[c,d] and Weihua Wang*[a]

[a.] Beijing National Laboratory for Condensed Matter Physics, Institute of Physics, Chinese Academy of Sciences, Beijing 100190, China

[b.] School of Physical Sciences, University of Chinese Academy of Sciences, Beijing 100190, China

[c.] Hefei National Research Center for Physical Sciences at the Microscale, CAS Key Laboratory of Strongly-Coupled Quantum Matter Physics, Department of Physics, University of Science and Technology of China, Hefei, Anhui 230026, China

[d.] Hefei National Laboratory, University of Science and Technology of China, Hefei, Anhui 230088, China

Emails: zfwang15@ustc.edu.cn; weihuawang@iphy.ac.cn

Methods

Growth of 1D FeQDI on Au(111)

The Au(111)/mica substrate was cleaned by repeated cycles of Ar^+ sputtering and annealing at 673 K for 30 minutes. Fe atoms were evaporated onto the clean substrates held at room temperature. Then 2,5-diamino-1,4-benzoquinonediimine (2HQDI) were deposited from a molecular beam evaporator (DODECON nanotechnology GmbH) at 383 K after rising the substrate temperature to 503 K. Finally, 1D FeQDI polymers were formed without post-annealing process.

Scanning Tunneling Microscopy

All experiments are performed in a scanning tunneling microscope (STM) system (Unisoku 1300) with a basic pressure better than 1×10^{-10} mbar. Unless otherwise specified, the STM and STS measurements are conducted at 4.9 K. The Pt/Ir tips are used in STM experiments. The bias voltage is applied to sample with respect to the tip. The differential conductance (dI/dV) signals are acquired using a lock-in amplifier with a sinusoidal modulation of 684 Hz at 10 mV.

First-Principles Calculations.

The first-principles calculations are performed based on density-functional theory (DFT) as implemented in the Vienna Ab initio Simulation Package (VASP),[1] using the projector augmented wave method and the strongly constrained and appropriately normed (SCAN)[2] meta-generalized-gradient-approximation functional. The plane-wave cutoff energy is set to 520 eV. The Monkhorst-Pack k-point mesh of 7 × 1 × 1 and the convergence criterion of 10^{-6} eV are used for all calculations. The vacuum layer of 18 Å is used to ensure the decoupling between neighboring slabs. The substrate is simulated by three layers of Au(111), and van der Waals corrections are applied using the DFT-D3 method.[3] During structural relaxation, the bottom-layer Au atoms are fixed, while all other atoms are fully relaxed with a force tolerance of 0.001 eV/Å. The Wannier-bands and orbitals are fitted using Wannier90 package.[4] Based on Tersoff-Hamann approximation, the experimental dI/dV images are simulated by theoretical LDOS maps with the real-space pixel averaging to include the tip effect.

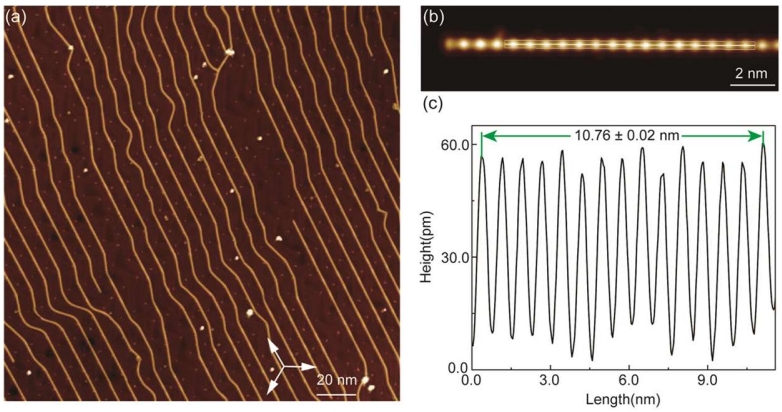

Fig. S1 (a) Large-scale STM image of FeQDI polymers on Au(111) substrate scanned at 77 K (-1.0 V and 10 pA). (b) Zoomed-in STM image of FeQDI polymer scanned at -0.2 V and 10 pA. (c) The lattice constant $a_0 \approx 0.77 \pm 0.02$ nm.

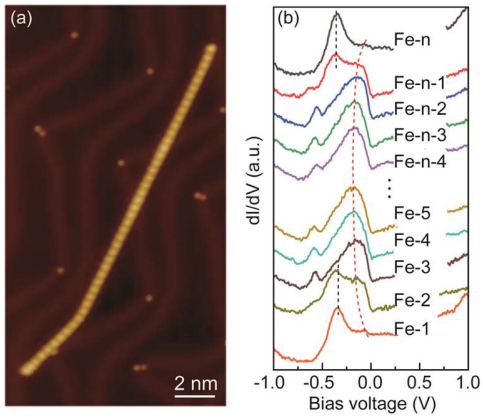

Fig. S2 (a) STM image of a FeQDI polymer on Au(111) substrate scanned at 77 K (-1.0 V and 10 pA). (b) The STS measured on Fe atoms along both ends of the FeQDI polymer in Fig. S2(a). The end state at Fe-1 (Fe-n) extends to Fe-2 (Fe-n-1) but gets neglectable on Fe-3 (Fe-n-2), and the bulk state extends to the end Fe atom at a higher energy. The curves are vertically shifted for clarity.

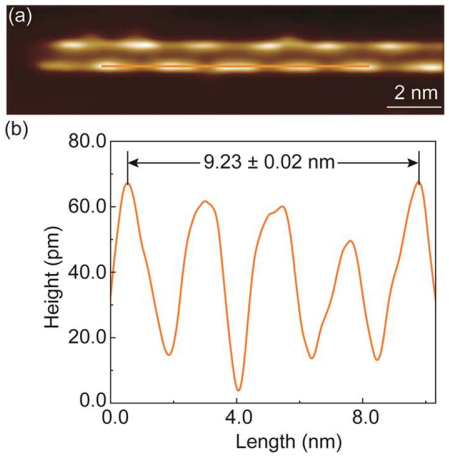

Fig. S3 (a) The dI/dV map at -0.6 V of FeQDI polymer. (b) The length of the one-dimensional moiré pattern marked by the orange line in Fig. S3(a). The period L = 2.31 ± 0.02 nm ≈ $3a_0$.

We analyzed the charge transfer between the monolayer 3× FeQDI supercell and the Au(111) substrate. Figure S4 illustrates the charge redistribution, where both top and side views are provided. In this analysis, we calculated the charge densities for three different systems: the charge density of the 3× FeQDI supercell on Au(111) ($\rho_{3\times FeQDI/Au}(r)$), the charge density of the Au(111) substrate ($\rho_{Au}(r)$), and the charge density of the freestanding 3× FeQDI supercell ($\rho_{3\times FeQDI}(r)$). We plot the charge redistribution by $\rho(r) = \rho_{3\times FeQDI/Au}(r) - \rho_{Au}(r) - \rho_{3\times FeQDI}(r)$. There is a net charge transfer of 0.74 e from per 3× FeQDI supercell to the Au(111) substrate, and the charge accumulation and depletion areas are indicated in red and green colors in Fig. S4, respectively. The side view clearly reveals charge depletion around the organic layer and charge accumulation near the Au surface.

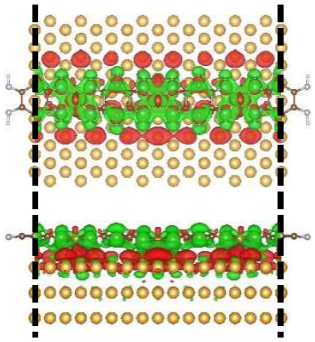

Fig. S4 The charge redistribution of 3× FeQDI supercell on the Au(111) substrate. The red and green colors indicate charge accumulation and depletion, respectively.

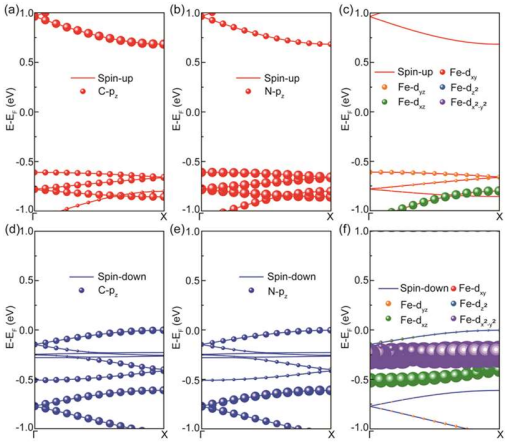

Fig. S5 The calculated orbital projection of band structure for freestanding FeQDI 3× supercell. The -0.15 V state observed in STS (Fig. 1(b)) is mainly contributed by the hybridization between Fe $3d_{x^2-y^2}$ and N $2p_z$ orbitals, and the -0.60 V state (Fig. 1(b)) in STS is given by the N $2p_z$ and C $2p_z$ orbitals of the QDI molecule.

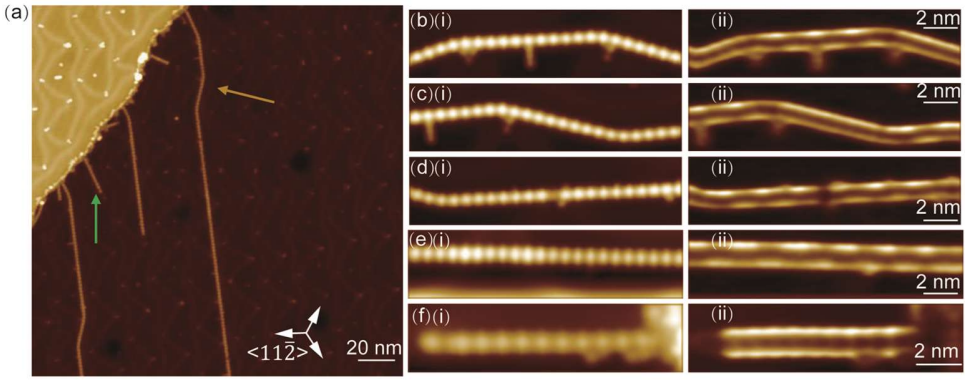

Fig. S6 (a) Large-scale STM image of FeQDI polymer (V = −1 V, I = 10 pA). (b-e) STM images (i) and d*I*/d*V* maps (ii) at -0.6 V of different segments in the same FeQDI polymer indicated by the yellow

arrow in Fig. S6(a). (f) STM image (i) and dI/dV map (ii) at -0.6 V of the FeQDI polymer indicated by the green arrow in Fig. S6(a).

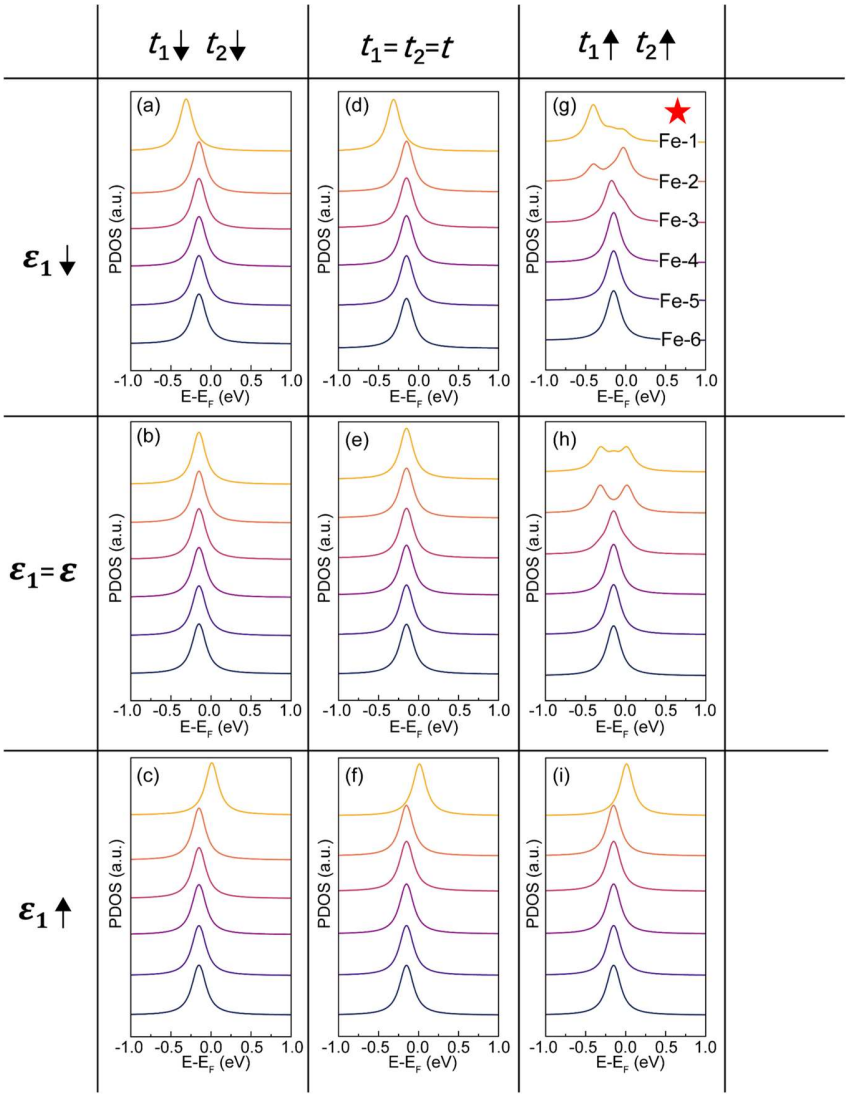

Fig. S7 Calculated PDOS according to different the hopping integrals (t_1, t_2) and on-site energy ε_1. (a-c) When shrinking the hopping integrals near the end (t_1 = 3.8 meV, t_2= 8 meV), regardless of whether the on-site energy increases (ε_1 =-0.31 eV) or decreases (ε_1=0.01 eV), there will be no difference on the electronic states between the second Fe atom and other Fe atoms inside the polymer, only the electronic state on the first Fe atom shift towards low or high energy. (d-f) When the hopping integral holds constant value along the whole polymer (t=t_1=t_2=15 meV), the adjustment of ε_1 also merely resulted in the movement of the first Fe electronic state. (g-i) With enlarged hopping integrals (t_1 = 150 meV, t_2= 75 meV), no matter how the ε_1 alters, two electronic states will appear on both the first Fe and the second Fe atoms. There is no difference between those two electronic states with ε_1=ε=-0.15 eV. By adding ε_1,

it enables two electronic states occupy different weights. Only by enlarging t_1 (t_2) and reducing ε_1 at the end of the polymer can the experimental results be fitted.

We use a finite segment of FeQDI on a single-layer Au(111) substrate to determine the adsorption configuration of the end Fe atom, while the atomic positions of the substrate are fixed throughout the optimization process. Figure S8 reveals the Fe-N bond length at the end is 0.02 Å longer than that in the FeQDI 3× supercell on Au(111), and the end Fe atom has a lower adsorption height on Au(111). The distance between the end Fe to Fe-2 is 0.4 Å shorter than that in the FeQDI 3× supercell, which may explain the enhanced hopping integral near the end of FeQDI.

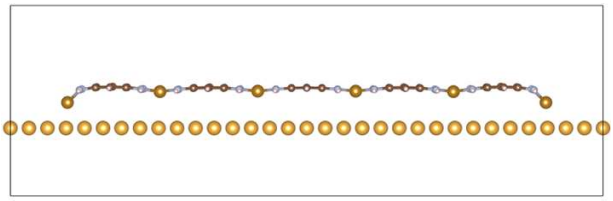

Fig. S8 Side view of the DFT optimized adsorption structure of a finite FeQDI segment on Au(111) substrate.

Different magnetic configurations are calculated to search the magnetic ground state, where the ferromagnetic (FM, Fig. S9(b)) and ferrimagnetic (FIM, Fig. S9(c)) configurations are considered. The energy of the FM state is 0.05 eV lower than that of the FIM state per FeQDI 3× supercell. Therefore, the FM state is the magnetic ground state. The magnetic moment of each Fe atom in the freestanding 3× FeQDI supercell is 2.40 μ_B. In the FeQDI 3× supercell with Au(111) substrate, due to the effect of the substrate, the magnetic moment of each Fe atom slightly decreases to 2.35 μ_B.

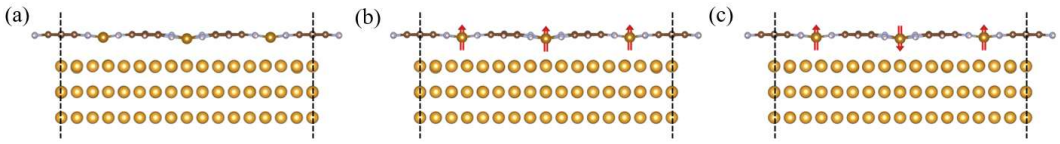

Fig. S9 (a) Non-magnetic configuration. (b) Ferromagnetic configuration. (c) Ferrimagnetic configuration. The energy differences between (a - c) relative to the ferromagnetic state are 3.22 eV, 0 eV, and 0.05 eV, respectively.

The absence of Kondo resonance on inner Fe atoms may be related to the following reasons: The magnetic moment of inner Fe (2.35 μ_B) is less than the end Fe (3.58 μ_B) due to their different coordination environments (The inner Fe is in a four-fold bis(diimino)-Fe coordination motif while the end Fe in a two-fold diimino-Fe motif.); the screening effect of itinerant electrons on the inner and end

Fe atoms are different due to their different adsorption height (The inner Fe has a higher adsorption height than the end Fe) and coordination environments; an extra energy is needed to flip the spin in inner Fe atoms due to the FM order in FeQDI, which prevents the Kondo resonance.

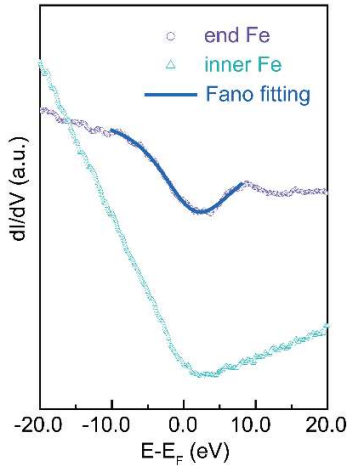

Fig. S10 The dip feature in the dI/dV curve of end Fe atom (purple circle) is fitted by the Fano function $f(x) = A\frac{[q+(x-x_0)/\Gamma]^2}{1+[(x-x_0)/\Gamma]^2} + B$, where x_0 and Γ are the width and energy of the resonance, q is the interference parameter. The fitting gives Γ≈7.03 mV and the Kondo temperature T_K ~ 56.7 $\pm$ 1.1 K ($\Gamma = \sqrt{(\pi k_B T)^2 + 2(k_B T_K)^2}$). The STS measured at the inner Fe atom (cyan triangle), there is no obvious magnetic signal. T = 4.9 K, lock-in:684 Hz, 0.5 mV.

References:

1. G. Kresse J. Furthmüller, *Physical review B,* 1996**, 54** (16), 11169.
2. J. Sun; A. Ruzsinszky J. P. Perdew, *Phys. Rev. Lett.,* 2015**, 115** (3), 036402.
3. S. Grimme; J. Antony; S. Ehrlich H. Krieg, *J. Chem. Phys,* 2010**, 132** (15).
4. A. A. Mostofi; J. R. Yates; G. Pizzi; Y.-S. Lee; I. Souza, et al., *Comput. Phys. Commun.,* 2014**, 185** (8), 2309-2310.